Pergamon

0301-9322(94)00043-3

Int. J. Multiphase Flow Vol. 20, No. 6, pp. 979–992, 1994

0301-9322/94 $7.00 + 0.00

DETAILED SINGLE SPRAY EXPERIMENTAL MEASUREMENTS AND ONE-DIMENSIONAL MODELLING

M. ST-GEORGES and J. M. BUCHLIN
von Karman Institute for Fluid Dynamics, 72 Chausseé de Waterloo, 1640 Rhode-St-Genèse, Belgium

(Received 15 September 1992; in revised form 29 April 1994)

Abstract—Detailed measurements are performed in liquid sprays with a laser velocimeter and the phase method; simultaneous measurements of drop size and velocity are obtained. The spray evolution is modelled on the basis of macroscopic balances, and the model developed reproduces with accuracy the spray behaviour. The measurements and modelling are oriented towards the analysis of the spray pollutant absorption potential, as a means to mitigate toxic gas release.

Key Words: pollutant dispersion, sprays, modelling, description, phase-Doppler method

1. INTRODUCTION

Accidental releases of toxic or flammable gases are a major problem for the chemical industry. Liquid sprays and liquid curtains are one of the available means to reduce the risks associated with such releases, their main advantages being flexibility, adaptability to very different operating conditions and a relatively low cost. A new field of interest is the physical absorption potential of the toxic products by liquid sprays, with the eventual addition of chemical reactants to enhance the absorption. This absorption effect might, in many cases, be more effective or more desirable than the dilution effect of a liquid curtain that simply mixes the toxic cloud with surrounding air.

The physical and chemical absorption of pollutants by liquid spray involve many phenomena and complex coupling: a special effort is devoted to study them in detail. A collaboration has been established between the von Karman Institute (VKI) and l'Institut des Technologies Chimiques of Lyon, France (ITC). The spray hydrodynamics are studied at the VKI while the ITC studies the absorption characteristics. The experimental conditions are carefully reproduced in both laboratories. The main objective is to be able to predict accurately the spray absorption efficiency and optimize its use.

The characteristics of a single spray are measured, and their evolution in the spray volume is established according to different operating parameters. A mathematical model is developed and compared with the experimental data.

2. SPRAY DESCRIPTION

A liquid spray is formed by the disintegration of a liquid sheet ejected from a nozzle, as shown by Dombrowsky & John (1963); the sheet becomes thinner as it moves away from the nozzle, and small perturbations from the surrounding air cause oscillations of the liquid film. The oscillations grow in amplitude until the film breaks down, first to filaments and then to droplets. After release, the droplets are under the action of the surrounding gas phase, and they experience momentum, mass and heat transfers. Interaction between droplets also exists that can range from slight modification of the local turbulence level to collision and disruption or coalescence. Work has been done to characterize these interactions by Ryley & Bennet-Cowell (1967), Adam *et al.* (1968) and Pasedag & Gallagher (1971).

Figure 1 shows a spray visualized by a laser tomography technique; the cone observed is formed by the spray droplets. On the left side, injection of smoke tracers with a rake shows the path followed by the air entrained inside the spray cone.

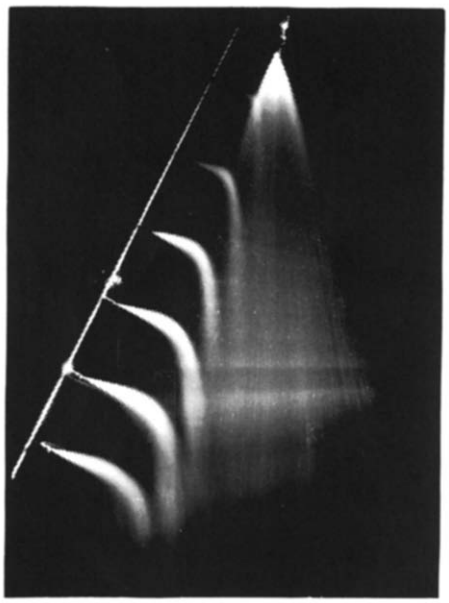

Figure 1. Visualization of a spray and its air entrainment.

The spray envelope is defined as the external limit of the region where the droplet–gas interactions take place; the initial angle of the envelope is the spray angle θ_0. As the gas and the droplets exchange momentum via the drag forces, the gas phase is accelerated and the droplets decelerated. The gas entrained inside the envelope drags the drops towards the centre of the spray, and thus the envelope cone tends towards a cylindrical shape; this hypothesis is confirmed by the evolution of the local measurements (section 4).

According to Buchlin (1988), the nozzle can be described with a few general parameters such as the flow number F_N in $m^3/s\sqrt{Pa}$, the discharge coefficient C_N and the initial spray angle θ_0. The size of the droplets produced by the nozzle can be represented by many distribution functions such as the Rosin–Rammler function, as listed in Lopez (1991):

$$\frac{dv}{dd} = \delta \frac{d_i^{\delta-1}}{\bar{d}^{\delta}} \exp^{(d_i/\bar{d})^{\delta}} \qquad [1]$$

where v is the cumulative volumetric fraction of drops smaller than the diameter d. The volumetric fraction of drops of diameter d_i is then dv/dd; dv is defined such that $\Sigma_0^{\infty} dv\, dd = 1$. $\bar{d}$ represents the size average and δ the dispersion around the mean. The parameters $\bar{d}$ and δ are obtained by a best fit calculation over experimental data; in general $2 < \delta < 4$.

3. SPRAY MODELLING

The present model is an extension of the model developed by Buchlin (1988) and follows the same philosophy. The basic hypotheses are the following:

- The flow is steady and no variation occurs across the spray: the properties are considered constant over a cross section (one-dimensional flow).
- The spray is axisymmetric around the z axis running from the nozzle in the direction of the liquid ejection.
- The drop size distribution is replaced by a finite number of size classes, the classes chosen are small enough to have similar behaviour for all the drops in each class.
- The spray is released in an infinite gas phase, initially at rest.
- The gas enters the spray envelope perpendicularly to the spray envelope, as seen in figure 1.
- The drops are spherical.
- The heat and mass transfers are neglected.

The single spray is modelled using the general parameters defined in the preceding section and the drop size distribution generated by the nozzle. The flow number; discharge coefficient and initial angle, together with the size distribution, define the initial conditions of the spray at ejection from the nozzle. The drop size distribution is generated from the Rosin–Rammler distribution function described above, specifying the average diameter, the dispersion parameter and the number of classes desired.

The evolution of the spray is simulated using a Lagrangian approach, following the evolution of single droplets.

3.1. Equation System

The local momentum and mass conversion equations give the evolution inside the gas–droplet interaction volume, and the trajectory of the drops on the envelope defines the envelope itself. The drops on the envelope are an artificial means of representing the evolution of the spray envelope: their diameter is fictitious, and their only purpose is to model the spray envelope evolution by their trajectories. They have a different velocity than the drops inside the envelope and their diameter is called the characteristic diameter of the drops on the envelope. Figure 2 displays the major dependent variables of the simulation.

Mass conservation balances

The mass conservation balance for the liquid phase, applied to each drop size class, leads to

$$\rho_{Li}^{*}\pi x_e^2 U_{di} = \rho_L L_{vi} \qquad [2]$$

where ρ_{Li}^{*} is the apparent density of the drop size class i, and it represents the liquid mass per unit volume of the gas–liquid mixture, x_e is the envelope radius, U_{di} is the velocity of the drops of class i, ρ_L is the liquid density and L_{vi} is the volumetric flow rate of the drops of class i. Summing over all the classes, we obtain

$$\rho_L^{*} = \frac{\rho_L}{\pi x_e^2}\sum_{n_d}\frac{L_{vi}}{U_{di}} \qquad [3]$$

where ρ_L^{*} is now the total apparent density. The mass balance for the gas phase, at a distance z from the nozzle, accounts for all the gas entrained at the envelope from the nozzle. It is expressed as

$$2\pi\rho_G\int_0^{z_s} x_e U_{Gc}\,\mathrm{d}l_e = \rho_G\pi x_e^2 U_{Ge} \qquad [4]$$

where ρ_G is the gas density, z_s is the position on the z axis, U_{Gc} is the entering velocity (at the envelope) of the gas and U_{Ge} is the average velocity of the gas inside the spray cone. The curvilinear length along the trajectory $\mathrm{d}l_e$ is such that, from geometrical considerations

$$\frac{\mathrm{d}z}{\mathrm{d}l_e} = \sin\beta \qquad [5]$$

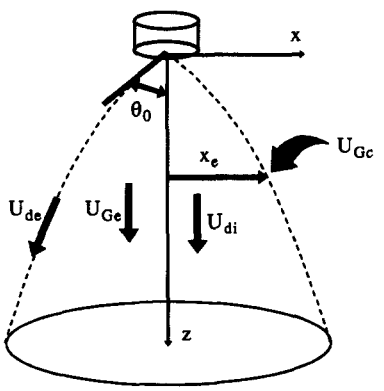

Figure 2. Main variables of spray simulation.

where β is the angle between the normal to the envelope and the vertical. Combining these last equations, we get

$$U_{Gc} = \frac{1}{2x_e} \sin\beta \frac{d(x_e^2 U_{Ge})}{dz} \quad [6]$$

This equation is best in terms of the gas phase momentum flow J_{Ge}, defined as

$$J_{Ge} = \pi \rho_G x_e^2 U_{Ge}^2 \quad [7]$$

and writing out explicitly the derivative of $x_e^2 U_{Ge}$

$$\frac{d(x_e^2 U_{Ge})}{dz} = x_e U_{Ge} \frac{dx_e}{dz} + \frac{1}{2\pi\rho_G U_{Ge}} \frac{dJ_{Ge}}{dz} \quad [8]$$

Substituting this final equation in [6], we finally obtain a relation in terms of the principal variables:

$$U_{Gc} = \frac{\sin\beta}{2} \left[U_{Ge} \frac{dx_e}{dz} + \frac{1}{2\pi\rho_G U_{Ge} x_e} \frac{dJ_{Ge}}{dz} \right] \quad [9]$$

Momentum conservation balances

The total momentum conservation balance along the z axis is performed on the gas and the liquid phases. It states that the momentum lost by the droplets must be recovered by the gas, plus or minus the gravity forces contribution applying to both phases. It is written as

$$\rho_L \sum_{n_d} L_{vi} \frac{dU_{di}}{dz} + \frac{dJ_{Ge}}{dz} = \pm \frac{dF_g}{dz} \quad [10]$$

The $\pm$ sign accounts for the gravity sign positive for a downward spray and negative for an upward spray, and F_g is the gravity force. Using [3] and accounting for Archimedes' force, the final form of the momentum conservation equation is

$$\frac{dJ_{Ge}}{dz} = \pm(\rho_L - \rho_G)\boldsymbol{g} \sum_{n_d} \frac{L_{vi}}{U_{di}} - \rho_L \sum_{n_d} L_{vi} \frac{dU_{di}}{dz} \quad [11]$$

where $\boldsymbol{g}$ is the gravity acceleration.

Drops inside the spray envelope

For the drops inside the spray envelope, one finds for every drop size class, using a force balance

$$\frac{dU_{di}}{dz} = \frac{1}{U_{di}} \left[\pm \left(1 - \frac{\rho_G}{\rho_L}\right) \boldsymbol{g} - \frac{3}{4} \frac{\rho_G}{\rho_L} \frac{C_{xi}}{d_i} |U_{dr_i}| U_{dr_i} \right] \quad [12]$$

The droplet drag coefficient and the drop diameter for the size class i are C_{xi} and d_i. The $\pm$ sign accounts again for the gravity sign: positive for a downward spray and negative for an upward spray. In this equation, U_{dr_i}, the relative velocity between the gas and the drops of class i, is given by

$$U_{dr_i} = U_{di} - U_{Ge} \quad [13]$$

and the drag coefficient is from the correlation for a spherical, rigid and isolated particle at steady state from Clift *et al.* (1978):

$$C_x = 0.36 + \frac{5.48}{Re^{0.573}} + \frac{24}{Re} \quad [14]$$

The Reynolds number Re is based on the relative velocity between the drop and the gas:

$$Re = \frac{dU_{dr}\rho_G}{\mu_G} \quad [15]$$

For the dense spray region close to the nozzle, the proximity of the drops influences the average drag coefficient: the drops travel in the wake of the preceding ones. We thus include in the model

the correlation for dense particulate flow from Wen & Yu (1966), where the modified drag coefficient C'_x is given in terms of the isolated particle one:

$$C'_x = C_x \epsilon^{-4.7} \quad [16]$$

where ϵ is the void fraction, the ratio of the volume occupied by the gas phase to the total volume, gas and liquid phases together.

Drops on the envelope

For the drops on the spray envelope, the relative velocity between the drops and the gas phase is, by definition

$$\overline{U_{dr_e}} = \overline{U_{de}} - \overline{U_{Gc}} \quad [17]$$

The variable U_{de} represents the velocity of the drops on the envelope and U_{dr_e} the relative velocity between the drops and the entering air; all velocities here are vectorial quantities as noted by the overbars. As shown by experimental data (figure 1), the gas enters the spray envelope perpendicularly to it. This geometric information gives the modulus of the relative velocity between the drops on the envelope and the entering gas (figure 3)

$$U_{dr_e} = \sqrt{U_{de}^2 + U_{Gc}^2} \quad [18]$$

The force balance of the drops on the envelope, projected tangential to the envelope then gives

$$\frac{dU_{de}}{dz} = \pm\left(1 - \frac{\rho_G}{\rho_L}\right)\frac{g}{U_{de}} - \frac{3}{4}\frac{\rho_G}{\rho_L}\frac{C_{xe}}{d_e}\frac{U_{dr_e}}{\sin\beta} \quad [19]$$

Where the drag coefficient C_{xe} uses the same correlation as for the drops inside the envelope, without correction for drop density. Here again, the $\pm$ sign stands for the gravity sign: the positive is for a downward spray and the negative is for an upward spray.

The following relation, derived from geometrical considerations, relates the angle of the envelope to the derivative of the envelope radius:

$$\cos\beta = \sin(\pi/2 - \beta) = \frac{1}{\sqrt{1 + \left(\frac{dz}{dx_e}\right)^2}} \quad [20]$$

The force balance of the drops on the envelope (figure 3), projected normal to the envelope, is written as

$$\rho_L V_{de} \gamma_{ne} = -F_{re_n} \pm (\rho_L - \rho_G) g V_{de} \sin\beta \quad [21]$$

where V_{de} is the volume of the drops on the envelope, γ_{ne} is the normal component of drop acceleration and F_{re_n} is the normal component of the drag force. As first developed

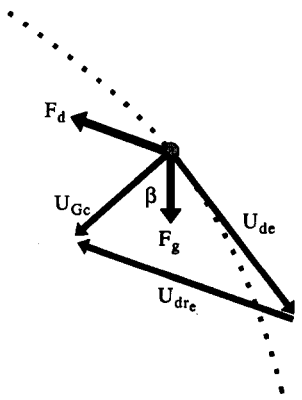

Figure 3. Force balance on the envelope.

by Rothe & Block (1977), the curvature radius of the drop trajectory r_c is related to the drop acceleration normal to the trajectory:

$$\frac{1}{r_c} = \frac{\gamma_{ne}}{U_{de}^2} \quad [22]$$

It can be rewritten as

$$\left[1 + \left(\frac{dx_e}{dz}\right)^2\right]^{-3/2} \frac{d^2x_e}{dz^2} = -\frac{\gamma_{ne}}{U_{de}^2} \quad [23]$$

The normal component of the drag force F_{re_n} is given by

$$F_{re_n} = \tfrac{1}{2} C_{xe} \rho_G A_{de} U_{dr_e}^2 \cdot U_{dr_e} \quad [24]$$

where $U_{dr_e}^n$ is the component of the relative velocity of the drops on the envelope projected normal to the trajectory and A_{de} is the cross-sectional area of the drops. As the velocity vectors U_{Gc} and U_{de} are perpendicular (see hypothesis), we have $U_{dr_e}^n = U_{Gc}$. Replacing and rearranging in [21] gives the final differential equation expressing the curvature of the trajectory of the drops on the envelope:

$$\frac{d^2x_e}{dz^2} = -\frac{3}{4}\frac{\rho_G}{\rho_L}\frac{C_{xe}}{d_e}\frac{U_{Gc}}{U_{de}}\frac{1}{\sin^3\beta}\sqrt{1 + \left(\frac{U_{Gc}}{U_{de}}\right)^2} \mp \left(1 - \frac{\rho_G}{\rho_L}\right)\frac{g}{U_{de}^2}\frac{\cos\beta}{\sin^3\beta} \quad [25]$$

Here the minus sign stands for a downward spray and the plus sign for an upward spray.

3.2. *Numerical Solution*

The equation system formed by [11], [12], [19] and [25] is a complete system of coupled ordinary differential equations of the first order. They include $n_d + 4$ equations and variables, namely

- the n_d drop velocities U_{di} for each drop size d_i
- the velocity U_{de} of the drops on the envelope
- the spray radius x_e and its first derivative dx_e/dz
- and the axial momentum of the gas phase J_{Ge}

The system of equations is solved using a z space marching Runge–Kutta scheme of the fourth order. The algorithm is coded in FORTRAN and has been used on a VAX-3500 and PC-AT. For an integration step of 1 mm and five drop size classes, the computational time is of the order of 1 minute per meter height on the PC. The simulation was found not to be too sensitive to the number of drop size classes, as more than five classes did not improve the precision (Lopez 1991).

The simulation results enable the calculation of some other very valuable quantities such as the gas velocity inside the spray envelope U_{Ge}, given by [7] and the gas volumetric flow rate $G_{ve} = \pi x_e^2 U_{Ge}$. Another is the total interfacial area A given by

$$A = \sum_{n_d} \frac{6L_{vi}}{d_i} \int_0^{z_s} \frac{dz}{U_{di}} \quad [26]$$

The results from the numerical simulation have to be compared with the experimental measurements to adjust and validate the model. The nozzle flow number, the operating pressure, the intitial spray angle and the droplet size distribution are inputs to the model. The characteristic diameter of the drops on the envelope d_e is a free parameter to be tuned with experimental data.

4. EXPERIMENTAL MEASUREMENTS

4.1. *Experimental Facility*

The experimental equipment used at the von Karman Institute is shown in figure 4. It is based on laser velocimetry to measure the drop velocity and on the phase method for the simultaneous drop size determination; see Bachalo & Houser (1984) for more details. The apparatus is the phase-Doppler particle analyzer (PDPA) from Aerometrics.

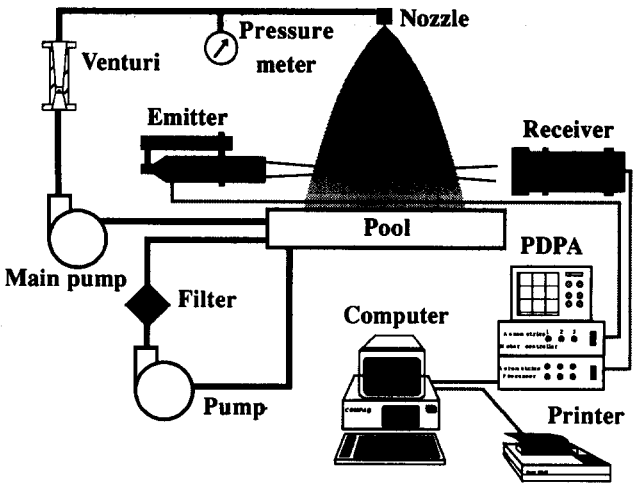

Figure 4. Experimental facility.

The spray nozzle is fed by a Moineau type volumetric pump delivering up to 10^{-3} m^3/s under 800 k Pa. It is actuated by a 1.5 kW electric motor and the flow rate is adjusted via a variable pulley and belt transmission. The water sprayed is collected in a pool 3 × 4 m wide and 0.3 m high. It is purified by an independent filtering system driven by a 1/3 kW centrifugal pump and using a diatomaceous earth filtering element capturing impurities larger than 1 μm.

The PDPA receiver faces the emitter and is at 30° from the laser beam axis; it gathers refracted light scattered forward. Both emitter and receiver were used with lenses of 1 m focal length, giving a probe volume of about 0.7 mm diameter and 1.5 mm length. With these lenses, drop diameters from about 10–2000 μm can be measured, but only a dynamic range of 1/35 can be obtained at once. This limit comes from the wide signal amplitude range between small and large drops, as it varies with the square of the drop diameter. Once the size range is adjusted, it is divided in a fixed number of 50 size bins.

The emitter and receiver are mounted on a displacement table that can traverse the whole pool length, and the nozzle is set in a slide enabling measurement heights from zero to about 2 m; it can also rotate. Using these three degrees of freedom, the whole spray volume can be investigated.

4.2. Measurement Strategy and Data Processing

The measurements are performed on a full cone pressure nozzle number 402.962 from Lechler; the spray angle is 30° and the orifice diameter is 6.25 mm. Measurements are taken in the spray volume at distances (heights) of 0.25, 0.45, 0.65, 0.85 and 1.05 m from the nozzle (figure 5). For

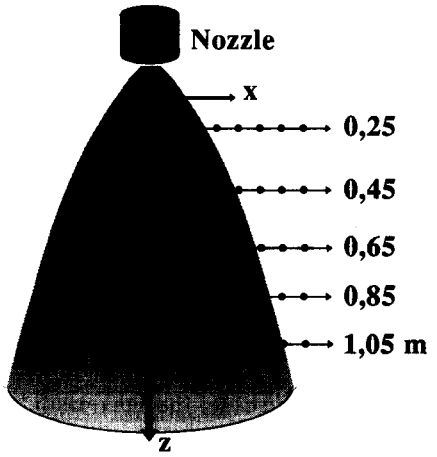

Figure 5. Measurement locations.

each height z, measurements are performed along the radius at about every centimeter. The spray has been verified to be quite symmetrical, and measurements could be taken only on one side of the axis.

Liquid phase measurement

The liquid phase measurement does not imply addition of any particle in the flow as the drops themselves are observed: the PDPA gives directly a local measurement of the spray drops. The characteristics measured are the local drop size distribution, the average diameters, the Rosin–Rammler distribution parameters, the velocity distribution, the average velocity, the velocity–diameter correlation, the flow rate, the drop density, the probe area P_A and the measurement time t_{mes}.

The local measurements are integrated numerically to obtain global characteristics of the spray, comparable to model results. The global drop size distribution is obtained by integrating the local drop counts per unit time and unit area $n_i/P_A t_{mes}$ over the spray cross section S. Thus the total number of drops of class i on a section, N_i, is given by

$$N_i = \int S\, 2\pi x \frac{n_i}{P_A t_{mes}}\, dx \qquad [27]$$

where x is the radius from the spray centerline. Calculating for every diameter d_i we obtain the global histogram.

The envelope is far more difficult to define on an experimental basis as there is no clear separation between the spray and the surrounding gas phase. The envelope location is defined using the flow rate measurements: it is said to contain 95% of the total flow rate. This definition is found to be practical and is consistent with the model definition.

The experimental spray angle θ_{0e} is obtained by the envelope definition at 0.25 m since the spray contraction so close to the nozzle is negligible. The average drop velocity of size class i on a spray section $\overline{U_{di}}$ is obtained by integration from the local measurements; the integration is performed as to be consistent with the model variable definition. It gives:

$$\overline{U_{di}} = \frac{\int_S 2\pi x \frac{n_i \overline{u_{di}}}{P_A t_{mes}}\, dx}{N_i} \qquad [28]$$

where $\overline{u_{di}}$ is the average velocity of drop size class i. The transit time t_{ti} is given by integration of the inverse of the average velocity as follows

$$t_{ti} = \int_z \frac{1}{U_{di}}\, dz \qquad [29]$$

Finally, the total interfacial area A, given by all the droplets present in the spray volume at any given time, is

$$A = \sum_{n_d} \int_z \int_S 2\pi x \frac{n_i \pi d_i^2}{P_A t_{mes} u_{di}}\, dx\, dz. \qquad [30]$$

Gas phase measurement

The direct gas phase measurement is not possible as the laser velocimetry requires the presence of particles. However, inside the spray, small drops are present in large amounts: the average velocity of the smallest drops can be considered very close to the gas phase velocity, as they have very little inertia and a high drag over inertia ratio. In the present experiment, all drops smaller than 20 μm are considered as good tracers. These measurements need other equipment settings than the liquid phase measurements, and are a completely independent set.

In the outer regions of the spray, specially outside of the envelope, tracer particles have to be added. Incense smoke was used for this purpose: the maximum size of the particles generated is of the order of 40 μm, and 90% of the smoke particles are smaller than 20 μm; they are unlikely to perturb the spray or the gas flow.

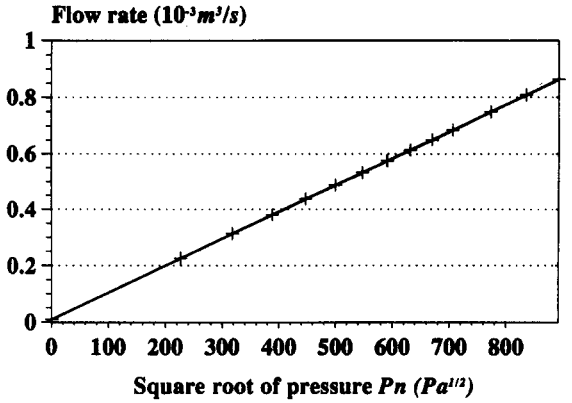

Figure 6. Nozzle flow rate calibration.

Having the local gas phase velocities, numerical integrations similar to the ones performed for the liquid phase gives the gas volumetric entrainment G_{ve}

$$G_{ve} = \int_S 2\pi x \overline{u_{Ge}}\, dx \qquad [31]$$

and the average gas entrainment velocity

$$U_{Ge} = \frac{G_{ve}}{\pi x_e^2} \qquad [32]$$

5. EXPERIMENTAL RESULTS

The nozzle flow calibration is done first, using a reservoir and a balance, measuring the time for a specific water mass. The result is plotted in figure 6.

The slope of the calibration curve gives the flow number $F_N = 9.7 * 10^{-7}\ m^3/s\sqrt{Pa}$. The relation agrees well with the theory as the relationship is linear on a semi-log graph (Buchlin 1988). The flow number is required for the simulation model.

Figure 7 shows the evolution of the average Sauter drop diameter across the spray, for a feed pressure P_n of 264 K Pa, at various heights. The mean diameter is quite uniform close to the nozzle, but a discrepancy builds up between the center and the outer regions as the distance increases. This variation is caused by the deviation of the small drops towards the center of the spray by the air entrained from the periphery: an increasing number of small drops are seen in the center of the spray, resulting in a decrease of the mean diameter, while only large drops are left at the periphery, causing an apparent increase of the mean diameter. This interpretation is confirmed by the global

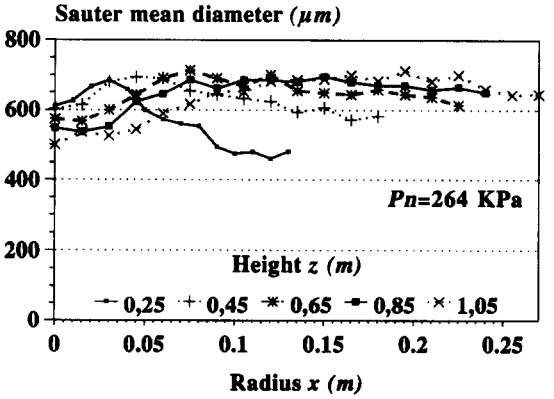

Figure 7. Drop size evolution across the spray at 264 kPa.

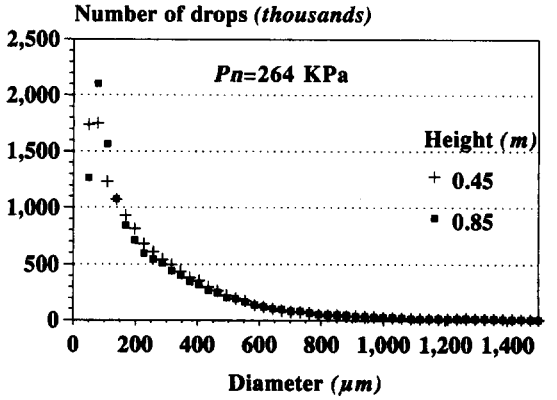

Figure 8. Global size distribution at 264 kPa, $z = 0.45$ and 0.85 m.

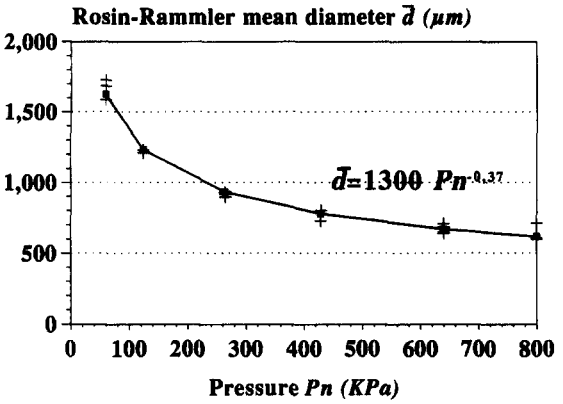

Figure 9. Variation of $\bar{d}$ with P_n.

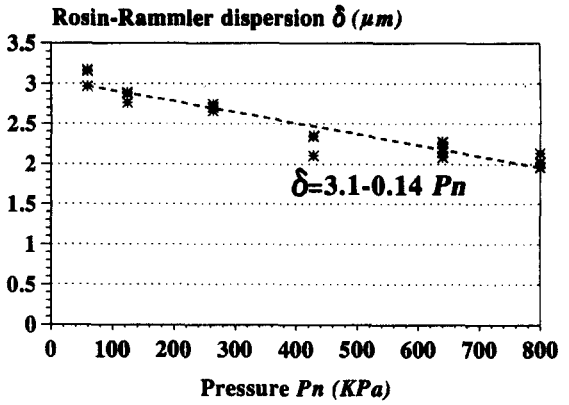

Figure 10. Variation of δ with P_n.

size distribution below, and it is in agreement with other published data by Chin *et al.* (1986) and Dodge *et al.* (1987). This drop size segregation is seen at every pressure and increasing with z.

Figure 8 shows the global drop size distributions over a whole spray section at 2.64 k Pa, 0.45 and 0.85 m from the nozzle. They are obtained by integration of the local PDPA measurements as explained in the preceding sections. The distribution is very similar from section to section: if droplet disruption or coalescence occurs, the overall effect is negligible here. Even in the local measurements, no evidence of droplet-interaction was visible. It does occur, but it is not a dominant factor in this spray.

The global drop size distribution does not vary with distance in the spray, but with the feed pressure P_n. Figures 9 and 10 show the variation of the Rosin–Rammler average diameter $\bar{d}$ and dispersion coefficient δ with P_n. The average diameter variation agrees quite well with a power law of the pressure, the exponent -0.37 being close to the theoretical -0.33 of Buchlin (1988). The dispersion coefficient seems to vary linearly according to our data. The Rosin–Rammler function used correlates quite well with the experimental data in the body of the spray, but not as well on the sides. This can be explained by the fact that the size distribution is largely modified by air entrainment in the outer region.

Figure 11 shows the envelope position, defined to include 95% of the flow rate; it varies with respect to the distance from the nozzle and the feed pressure. The envelope extends further as the pressure increases but stabilizes for the high pressures: from 264 to 800 k Pa, it does not vary significantly. The envelope position at 0.25 m leads to the spray initial angle definition shown in figure 12: as expected, it is almost constant for operating pressures between 264 and 800 k Pa. The average angle is 37.5°, somewhat higher than the nominal manufacturer angle of 30°. The experimental initial angle is used as input for the model.

The average drop velocity over the spray section, as a function of the drop size and distance from the nozzle at 264 k Pa, is plotted in figure 13. Again it is obtained from integration of the

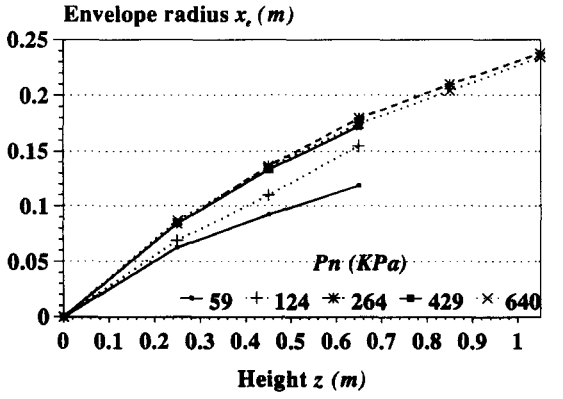

Figure 11. Envelope position.

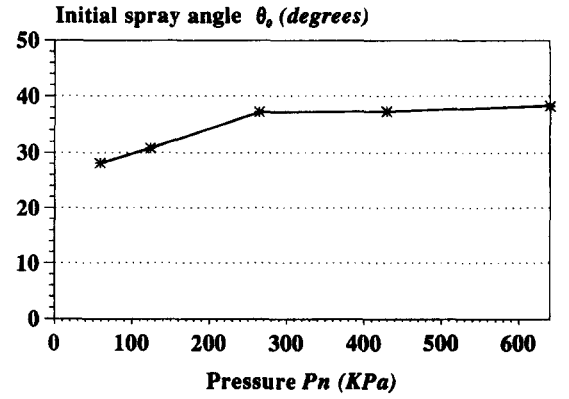

Figure 12. Initial spray angle θ_0.

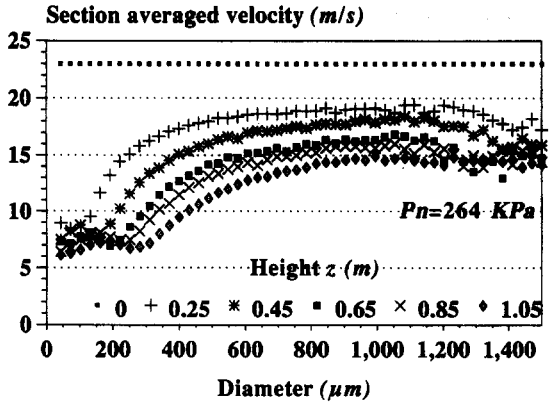

Figure 13. Global d–U_{di} correlation.

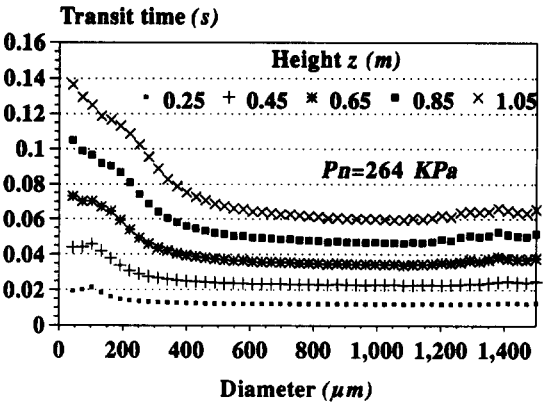

Figure 14. Average transit time.

local measurements as explained above; it shows decreasing average velocities for increasing z and an increase in the diameter–velocity correlation. The top line is the ejection velocity, obtained analytically from the Bernoulli equation, and is shown for comparison. The small drops are slowed down much faster than the larger ones, building up an important velocity difference between them. The larger the drop, the smaller is the deceleration effect from the gas phase.

Integration of the inverse of the velocity leads to the drop transit time as a function of drop size and distance from the nozzle. The transit time is the duration of the intimate contact between the drop and the gas, thus giving a direct indication of the pollutant absorption time. Figure 14 shows the transit times obtained at a pressure of 264 k Pa. It increases as z increases, but more quickly for the small drops than for the larger ones, as a result of the drop slow down discussed in the previous paragraph. These results show that the small drops have the greatest potential for pollutant absorption as they have the greatest transit time. Moreover, they are extremely numerous and they offer the greatest interfacial area per unit flow rate.

Figure 15 shows the distribution of the interfacial area obtained from [26]. It displays a two-dimensional sheet of the spray, extending from the axis of symmetry to the edge of the spray. The interfacial area is multiplied by $2\pi x$, where x is the local radius, to account for the annular section where this area applies. This transformation shows the distribution of the interfacial area in a more realistic way, and the units are m^2 of interfacial area per m^2 of spray section in the z–x plane. We observe that the maximum local interfacial area is at a radius higher than the maximum drop density because the annulus surface grows fast as the radius increases.

The total interfacial area, as a function of the distance from the nozzle and the operating pressure, is shown in figure 16. The interfacial area is increasing with increasing pressure, although the transit time of the droplets decreases as their travel velocity increases, because this effect is largely overcome by an increase in the flow rate and a decrease in the size of the droplets.

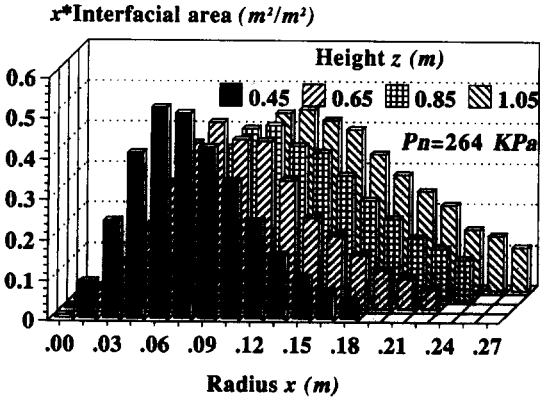

Figure 15. Interfacial area distribution.

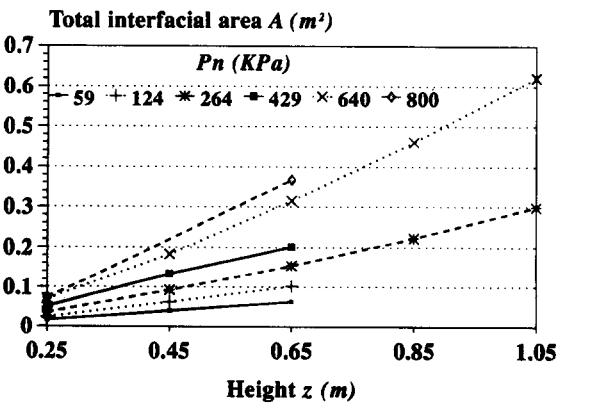

Figure 16. Total interfacial area.

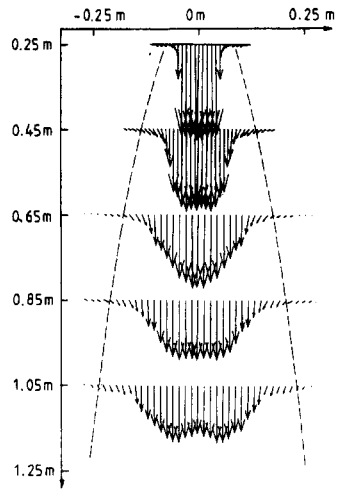

Figure 17. Gas velocity vectors at 264 kPa.

The two-dimensional gas phase measurement is performed using other settings for the PDPA, focusing on the drops smaller than 20 μm; this leads to figures 17 and 18. The first figure shows the velocity vectors in the spray for a pressure of 264 kPa: in this figure, the centreline velocity at 0.25 m from the nozzle corresponds to 12.5 m/s. The velocity of the gas is quite uniform in the centre of the spray, and the direction of the entrained air in the proximity of the envelope can be appreciated; it approaches the envelope approximately perpendicularly and turns down short after spray penetration. This result is in very good agreement with the visualization of figure 1. In figure 18, the total flow rate of entrained air is shown as a function of the operating pressure and the spray height; it increases almost linearly with the spray height and the pressure.

6. MODEL–EXPERIMENT COMPARISON

The initial conditions of the spray measured are injected in the numerical model: spray angle, flow number, drop size distribution and operating pressure. The simulations are then compared to the measurements. The number of drop size classes for the simulation has been set at five; runs with ten classes were not found to be much more accurate but twice as costly in terms of computational time.

The characteristic diameter of the drops on the envelope is chosen to obtain the best possible fit with the experimental envelope evolution. The model predictions are quite sensitive to the envelope characteristic diameter: it has to be carefully determined. Nevertheless, it is seen to be independent of the pressure, as is the spray angle (Nieuwkamp 1985), suggesting that it is

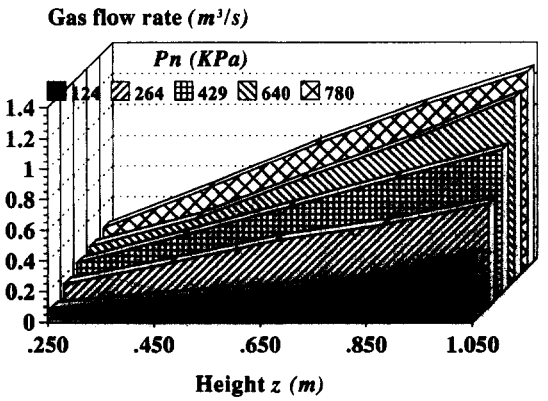

Figure 18. Entrained gas flow rate.

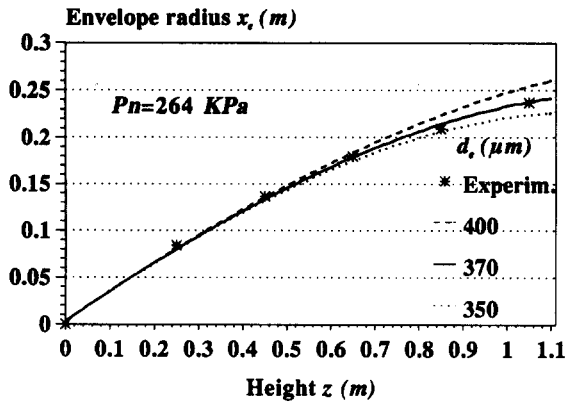

Figure 19. Envelope positon comparison at 264 kPa.

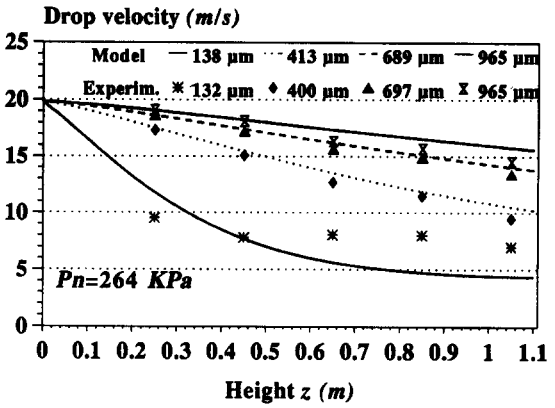

Figure 20. Drop velocity comparison at 264 kPa.

characteristic of the nozzle rather than the drop size distribution. This may come from counterbalancing effects; the spray drop size decreases as the pressure increases but the ejection velocity increases as well as the droplet density. Figure 19 shows a comparison between simulations and experiments; a very good agreement is achieved for a characteristic diameter of drops on the envelope of 370 μm.

The simulations also point out a high sensitivity of the model to the initial conditions: accurate nozzle characteristics are mandatory for correct simulation of the spray evolution, and the manufacturer's data are often sparse and not accurate enough.

Comparison between the predicted drop velocity and the measured one is shown in figure 20 for four size classes; the measurements are averaged over the spray section. The model acceptably predicts the velocity of the medium and large drops, but predicts too low velocities for the smallest ones. This could be due to a bias in the measurements; the probability of rejecting a signal from a small particle is greater if the particle is slow and takes a long time to cross the probe area; more of the slow particles are rejected, resulting in a too high velocity average. Investigation is underway to quantify this bias.

The total interfacial area predictions are in relatively good agreement with the experimental values, as shown in figure 21; the divergence at large distances is due to the difference in the velocity of the small drops noticed previously, as they contribute greatly to the interfacial area; the experimental area is slightly under-estimated. Figure 22 shows a comparison of the entrained gas flow rate; a very good agreement is found for all pressures.

7. CONCLUSION

The laboratory, equipped with a laser velocimeter using the phase difference for the simultaneous measurement of the drop diameter, is well suited for the study of sprays. The spray produced by

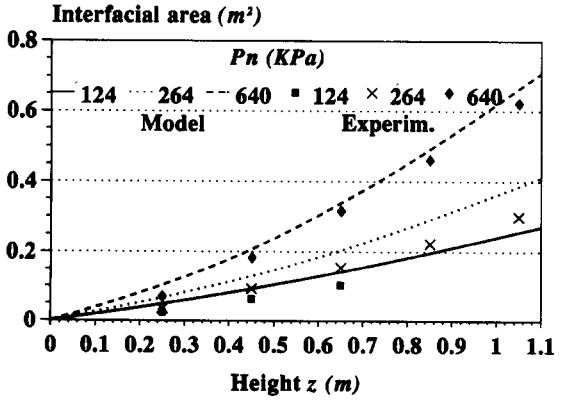

Figure 21. Interfacial area comparison.

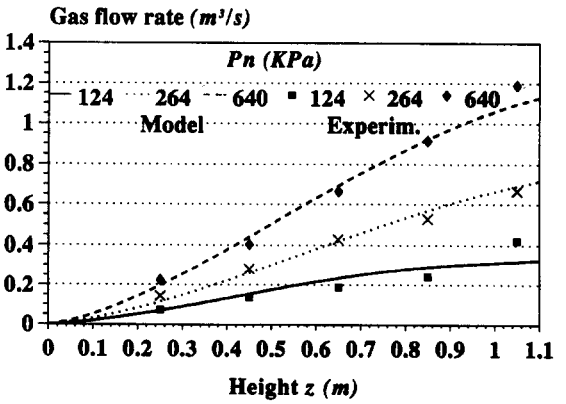

Figure 22. Gas flow rate comparison.

a full cone pressure nozzle was studied in detail. Entrainment of the small drops towards the centre of the spray by the incoming air is observed, but no evidence of droplet disruption or coalesence has been clearly seen. The Rosin–Rammler function was used successfully to correlate the measured drop size dispersion. The spray initial angle is seen to be independent of pressure, and the spray envelope evolution has been obtained. From the local measurements the drops average transit time and contact area with the gas phase are finally obtained. The gas phase velocity can be measured using a particular setting of the equipment, and air entrainment is quantified.

The spray model developed, although simple, reproduces with good accuracy the global evolution of the spray: drop velocities, interfacial area, transit time and air entrainment are well predicted. This is a useful basis for the development of a physical and chemical absorption model to predict the absorption potential of the spray.

Future works includes extension of the model for hollow cone and flat fan sprays, and the study of sprays in an atmospheric curtain, with interaction between sprays and wind.

Acknowledgements—The von Karman Institute wishes to express its gratitude to the industrial companies that sponsored this research: Comhurex, Gaz de France, Institut Francais du Petrole, Rhone-Poulenc, Societé Nationale Elf-Aquitaine (Atochem-Norsolor), Societé Nationale des Poudres et Explosifs and the French Ministry of Environment for interest shown in this project.

REFERENCES

ADAM J. R., LINDBLAD, N. R. & HENDRICKS C. D. 1968 The collision, coalesence, and disruption of water droplets. *J. Appl. Phys.* **39,** 5173–5180.

BACHALO, W. D. & HOUSER W. D. 1984 Phase doppler spray analysis for simultaneous measurements of drop size and velocity distribution. *Opt. Engng* **23,** 583–590.

BUCHLIN, J.-M 1988 Liquid sprays. Course Note 131/EA, von Karman Institute for Fluid Dynamics, Belgium.

CHIN, J. S., NICKOLAUS, D. & LEFEBVRE, A. H. 1986 Influence of downstream distance on the spray characteristics of pressure-swirl atomizers. *J. Engng Gas Turbines Power* **108,** 219–224.

CLIFT, R., GRACE J. R. & WEBER, M. E. 1978 *Bubbles, Drops and Particles.* Academic Press, New York.

DODGE, L. G., RHODES, D. J. & REITZ, R. D. 1987 Drop-size measurement techniques for sprays: comparison of malvern laser diffraction and Aerometrics phase/doppler. *Appl. Optics* **26,** 2144–2154.

DOMBROWSKI, N. & JOHNS W. R. 1963 The aerodynamic instability and disintegration of viscous liquid sheets. *Chem. Engng Sci.* **18,** 203–241.

LOPEZ, J.-P. 1991 Les rideaux de fluides appliqués au contrôle des rejets accidentels de gaz dangereux: modélisation et dimensionnement. Ph.D. thesis, Université Claude Bernard-Lyon 1, France.

NIEUWKAMP, W. C. 1985 Flow analysis of a hollow cone nozzle with potential flow theory. In *International Conference on Liquid Atomization and Spray Systems*, Vol. 1, pp. IIIC/1/1–IIIC/1/9.

PASEDAG, W. F. & GALLAGHER, J. L. 1971 Drop size distribution and spray effectiveness. *Nucl. Technol.* **10,** 412–418.

ROTHE, P. H. & BLOCK, J. A. 1977 Aerodynamic behaviour of liquid sprays. *Int. J. Multiphase Flow* **3,** 263–272.

RYLEY, D. J. & BENNET-COWELL, B. N. 1967 The collision behaviour of steam-borne water drops. *Int. J. Mech. Sci.* **9,** 817–833.

WEN, C. Y. & YU, Y. H. 1966 A generalized method for predicting the minimum fluidization velocity. *AICheJl* **12,** 610–612.